NJC

ROYAL SOCIETY OF CHEMISTRY

PAPER

View Article Online
View Journal | View Issue

Cite this: *New J. Chem.*, 2021, 45, 6273

The fabrication and characterization of a supramolecular Cu-based metallogel thin-film based Schottky diode†

Vivek Kumar,[a] Rishibrind Kumar Upadhyay,[b] Daraksha Bano,[a] Subhash Chandra,[a] Deepak Kumar,[a] Satyabrata Jit[b] and Syed Hadi Hasan*[a]

Received 25th January 2021,
Accepted 8th March 2021

DOI: 10.1039/d1nj00394a

rsc.li/njc

In the present study, a stable supramolecular Cu(II)-metallogel has been synthesized based on copper(II) acetate monohydrate and succinic acid, engineered as a low-molecular-weight organic gelator. The mechanical assets of the Cu–H_4L metallogel have been explored through a rheological investigation. Further, the aggregation of the synthesized metallogel has been well established *via* several experiments using Job plots and ESI-MS. Apart from this, the morphology of the synthesized supramolecular metallogel was scrutinized *via* FESEM, TEM, and AFM studies, revealing the self-assembled thread-like morphology of the Cu–H_4L metallogel. The functional group, elemental composition, crystalline behaviour, and thermal stability of the Cu–H_4L metallogel were probed *via* FT-IR, XPS, P-XRD, and TGA studies, respectively. The optical properties of the Cu–H_4L metallogel reflected its semiconducting nature. Thus, based on the semiconducting properties of the Cu–H_4L metallogel, we have successfully fabricated an active electronic device: a 'Schottky diode'.

1. Introduction

Investigation of gel-like soft resources has been of emerging interest because of their many applications extending from research to manufacturing areas.[1,2] Supramolecular gels have potential applicability in several fields including catalysis,[1] lithography,[2,3] optoelectronic devices,[3] electrochemical devices,[4] chemo-sensors,[5] cell culturing,[5] biomedicine,[6,7] medical diagnostics,[7] drug delivery,[8,9] wastewater treatment,[10] tissue engineering,[9] sensor science,[11] and semiconductors.[12] During the last two decades, the discovery of a new low molecular weight conducting metallogelator has been accompanied by a decisive development in the field of coordination polymers and metal–organic frameworks that may allow the fabrication of novel metallogels with challenging features.[13] In recent research, conductive metallogels have turned out to be captivating functionalized materials[14] because of their advancement in optical, electronic, and electrical devices.[15]

However, the synthesis of conductive metallogels, having self-healing property to fabricate electronic devices, is still a challenging task in the scientific community.[11] Metal–semiconductor (MS) junctions are the crucial part of effectively all semiconducting optoelectronic devices.[16] The formation of such an MS junction interface greatly affects the quality and performance of devices.[17] During the last few years, there has been considerable attention paid to experimental studies of MS-based Schottky barrier diodes (SBDs). The present disclosure generally relates to SBDs that have a metal for the Schottky layer and the semiconductor material for the drift layer is selected to provide a low barrier height Schottky junction between the drift layer and the Schottky layer. Schottky barrier height is a key property of the MS interface of SBDs, which governs the electronic transfer across the interface,[18] and the electrical characteristics such as voltage drop and switching speed of such devices are dependent on the current transport behaviour through the structure of the MS interface. SBDs provide great advantages over a traditional analogous p–n diode as they have lower barrier height; thus, a lower voltage is required to turn on the device.[19]

Taking all these considerations into account, we have examined the semiconducting properties of a synthesized metallogel (Cu–H_4L) and successfully fabricated a MS junction based thin-film device (Ag/Cu–H_4L) at room temperature (RT). The calculated direct energy band gap of the metallogel was ~3.06 eV, which showed the improved optical properties over those of previously reported literature.[12,20] The *I–V* characteristics of the Ag/Cu–H_4L based thin-film device display a nonlinear rectifying behaviour, suggesting the formation of a

[a] *Department of Chemistry, Nano-materials Laboratory, IIT BHU, Varanasi-221005, India. E-mail: shhasan.apc@itbhu.ac.in; Tel: +91 9839089919*
[b] *Department of Electronics Engineering, IIT BHU, Varanasi-221005, India*

† Electronic supplementary information (ESI) available. See DOI: 10.1039/d1nj00394a

SBD. The important SBD parameters of the fabricated device such as rectification ratio, ideality factor, and barrier height were extracted from current–voltage characteristics by Cheung's method. It is, therefore, of critical importance to reduce the barrier height of the Ag/Cu–H_4L interface to improve the on-state voltage drop in Ag/Cu–H_4L devices. Moreover, from extensive studies it has been found that our designed semiconducting thin-film based SBD has the advantages of enhanced electrical conductivity, high chemical stability and low-cost production process.

2. Experimental

2.1. Materials

Succinic acid, hydrazine hydrate, salicylaldehyde, copper acetate monohydrate and solvents were acquired from S.D. Fine Private Ltd. Throughout all the experiments, the chemicals were used without additional purification.

2.2. Characterization

The UV-visible spectra were obtained with a Thermo Scientific EVOLUTION 201 spectrophotometer. A PerkinElmer Spectrum spectrophotometer was used for FT-IR characterization. ^{1}H NMR study was conducted with a Bruker AVANCE III HD 500 spectrometer. A Micromass MS Technologies SCIEX X500R QTOF was used for recording the ESI-MS spectra. A Tecnai G2 20 TWIN was used for capturing TEM micrographs. Rheology of the metallogel was investigated with an Anton Paar MCR 702 twin drive rheometer. The SEM images were collected with an EVO scanning electron microscope (MA15/18). Powder XRD data were accumulated in the range of angle 2θ = 10–90° using a Rigaku MiniFlex 600 Detector D-tex Ultra.

2.3. Synthesis of the gelator (H_4L)

The reported ligand[18] was synthesized by the reaction mixture of methanolic solution of succinic acid (1.00 g, 8.46 mmol) and a catalytic amount of concentrated sulphuric acid which was refluxed overnight. Afterwards, a clear solution of dimethyl succinate was obtained with a pleasant smell. Further, this methanolic mixture was refluxed with hydrazine hydrate (863 mg, 16.9 mmol) under an in-situ condition for 6 hours, leading to white crystals of succinoyldihydrazine, which were isolated by filtration. Then, dihydrazone was prepared by reacting a solution of succinoyldihydrazine (1.0 g, 6.8 mmol) with salicylaldehyde in methanol (1.67 g, 13.6 mmol). Subsequently, a white precipitate was obtained at RT, which was dried and collected after washing with methanol, resulting in a yield of 82% of gelator.

^{1}H NMR of the synthesized gelator was conducted in [D_6] DMSO. ^{1}H NMR (500 MHz, [D_6] DMSO, 25 °C): δ = 11.72 (s, 1 H, –OH); 11.29 (s, 1 H, –OH); 11.17 (s, 1 H, NH); 10.15 (s, 1 H, NH); 8.35 (s, 1 H, CH═N); 8.28 (s, 1 H, CH═N); 6.85–7.65 (m, 8H, Ar-H); 2.93 (m, 2 H); 2.50 (m, 2 H).

2.4. Synthesis of the metallogel

In a typical synthesis process, the gelator H_4L (14 mg, 0.04 mmol) was dissolved in DMF (0.6 mL) in a vial. Then a freshly prepared $Cu(OAc)_2$ (8.0 mg, 0.04 mmol) solution in DMF (0.4 mL) was added in one shot. A green-coloured stiff gel was formed instantly at RT without any external mechanical influence. The thus formed gelatinous material was examined by conventional inverted vial method, which confirmed the sustainability of the gel.

2.5. Device fabrication

For MS junction device fabrication, indium doped tin oxide (ITO)-coated glass substrates (15 × 15 mm^2) were ultrasonically cleaned using standard wet cleaning successively in soap solution for 20 minutes, deionized water for 15 minutes, acetone for 10 minutes, and isopropanol for 10 minutes, before finally being treated *via* plasma cleaning in the presence of argon for 20 minutes.[19,20] Initially, supramolecular Cu-based metallogel was deposited on the ITO-coated glass substrate and annealed at 100 °C for 30 min. In the second step, ~80 nm thickness of metal (Ag) was deposited for a contact electrode by using a thermal evaporator unit. The evaporated metal (Ag) formed circular dots of 1 mm in radius on the top of the semiconductor device using a shadow mask technique.[20] The thicknesses of the Cu–H_4L gel layer (~200 nm) were measured using an F20 Filmmetrics (USA) instrument.[20]

3. Results and discussion

To synthesize the metallogel, first, we designed the gelator (H_4L), derived from succinic acid, as shown in Scheme 1.

The direct gelation test was performed by adding different metal cations such as Cd^{2+}, Co^{2+}, Zn^{2+}, Cu^{2+}, Ni^{2+}, Pb^{2+}, Mn^{2+}, Fe^{2+}, and Sn^{2+} into the as-synthesized gelator (H_4L) in DMF, as shown in Fig. S1 (ESI). It can be noticed that among these metal cations, specifically $Cu(OAc)_2$ was capable of forming a gel with gelator H_4L. The morphological characteristics of the synthesized metallogel were investigated by SEM, TEM, and AFM analyses.

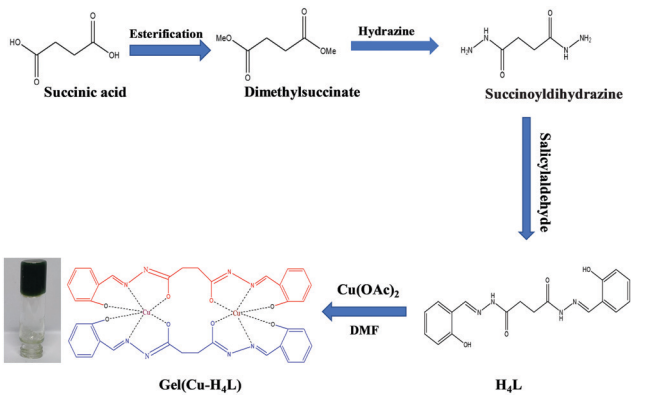

Scheme 1 The synthetic scheme of the Cu–H_4L based metallogel.

3.1. UV-visible study

A UV-visible absorption spectroscopy investigation showed the complexation behaviour of the gelator with Cu(II) in DMF. As shown in Fig. 1, a UV-visible titration experiment was performed between gelator and Cu(II) metal ion by varying the metal-to-gelator ratio. The UV-visible spectrum of the gelator exhibited two sharp bands at 281 nm and 290 nm, which may be due to the π–π* transition. A less intense band at 322 nm corresponds to the n–π* transition.[21] The alternate band appeared at 281 nm, and that at 290 nm was due to the unlike planarity of the ligand.[22] On further multiple inclusions of $Cu(OAc)_2$ (1×10^{-3} M, DMF, 25 °C) to this solution, a substantial change was observed: the vanishing of the band at 322 nm and a new peak appeared at 380 nm, indicating that Cu^{2+} formed a complex with the gelator.[22] And the shift of wavelength ($\Delta\lambda$ = 62 nm), with the origin of an isosbestic point at 342 nm, specifies the existence of an equilibrium state throughout the complexation of gelator and Cu(II) ion. In the range of 1–1.2 equivalent of gelator/Cu(II), the appearance of a saturation point indicates the possibility of 1 : 1 coordination, which was further confirmed by Job's plot for [Cu(II)]/[Cu(II)] + [gelator] *vs.* absorbance monitored at 380 nm.

3.2. FT-IR analysis

The gelator H_4L showed (Fig. 2a) a strong broad band in the region of 3200 cm^{-1} and a hump at 3430 cm^{-1}, which arise due to the vibration of secondary –NH groups and naphtholic/phenolic –OH groups, respectively.[23] The FT-IR spectrum of the gelator also showed bands at 1665 cm^{-1} and 1567 cm^{-1} due to the (>C=N) and (>C=O) vibrations respectively.[18] As shown in Fig. 2b, the spectrum of the xerogel has a strong broad band in the region of 3436 cm^{-1}, which suggests the –OH band of lattice/coordinated water molecules.[18] The synthesized xerogel did not show any band in the region of 3200 cm^{-1} (–NH); that is attributed to the enol form in the complex.[18] In the FT-IR spectrum of the xerogel, >C=N and >C=O bands shifted to 1610 cm^{-1} ($\Delta\nu$ = 55) and 1505 cm^{-1} ($\Delta\nu$ = 62 cm^{-1}) compared to those of the gelator, advocating the involvement of >C=N and >C=O in complexation.[24] Thus, it could be expected that coordination of Cu^{2+} with the synthesized gelator (H_4L) occurs through the O, N, O linkage.

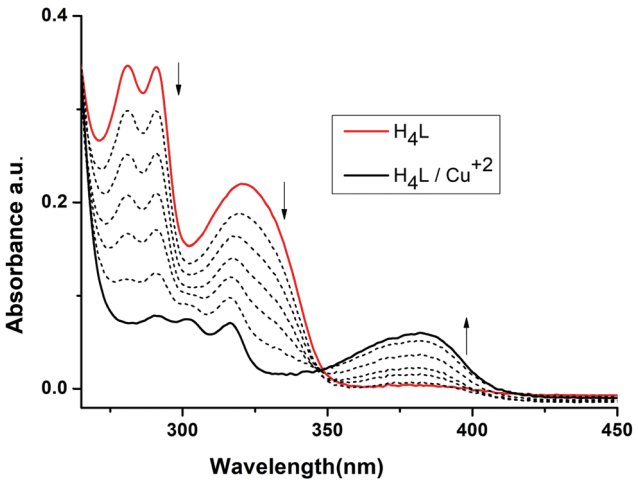

Fig. 1 The UV-visible titration evaluation of H_4L alone (1×10^{-5} M, DMF, red line) and with $Cu(OAc)_2$ (1×10^{-3} M, DMF, black dotted lines).

3.3. Morphological study

The morphological characteristics of the synthesized metallogel were investigated by FESEM, TEM, and AFM analyses. The microstructural pattern of supramolecular Cu–H_4L based metallogel was explored by FESEM. The interconnected collection of thread-like nanofiber morphology of the gel has an average size ~1 μm, as shown in Fig. 3a. Morphological properties of the metallogel dictate the compactness of thin intertwined nanofibers. The network formation of nanofibers was confirmed by the TEM and AFM analyses of the metallogel, as revealed in Fig. 3b and c, respectively. This result revealed the formation of an intermingled network of nanofibers along with an average diameter of ~6 nm and lengths of several micrometers. Supramolecular noncovalent interaction between the Cu(II) source and the gelator H_4L in DMF could be effective for the self-assembly growth which leads to the Cu(II) ion based stable metallogel.

The powder X-ray diffraction pattern of the xerogel, formed using Cu–H_4L metallogel, in the 2θ range of 10° to 90° showed a common broad diffraction peak at 21.6° indicating the amorphous behaviour of the gel,[25–27] as shown in Fig. S2 (ESI†).

Thermogravimetric analysis (TGA) is a substantial method to determine the thermal stability of a material, including polymers.[28] In this technique, a change in the weight of a sample is measured with respect to an increase in temperature. TGA measurement was carried out on 15.8 mg of the Cu(II)-H_4L xerogel at a heating rate of 10 °C min^{-1} in a nitrogen atmosphere using a thermogravimetric analyzer (instrument model: TGA-50, Shimadzu (Asia Pacific) Pte Ltd). The continuous weight loss and temperature were analyzed thoroughly after recording (Fig. 4). The result showed that up to 200 °C not as much weight loss was observed; this indicates the thermal stability of the gel material when it is exposed to heat at 200 °C.

The oxidation state of Cu was determined by XPS. In the high-resolution XPS spectrum of Cu 2p of the synthesized xerogel, two peaks were observed at 936.1 and 956.0 eV, along with two satellite peaks at 942.7 and 946.2 eV, which correspond to the $2p_{3/2}$ and $2p_{1/2}$ of copper, confirming the presence of Cu(II) state[29] (Fig. 5). The high-resolution XPS spectra[30,31] of C 1s, N 1s, O 1s, and Cu 2p of Cu–H_4L metallogel were obtained, as shown in Fig. S3 (ESI†).

3.4. Mass spectral analysis

The Job's plot method (Fig. 6a) indicates that the stoichiometric ratio of the complex formed during gelation between Cu^{2+} and gelator H_4L in DMF solvent is 1 : 1, under experimental conditions. This was further confirmed by ESI-MS spectral analysis of the diluted metallogel. As shown in Fig. 6b, the molecular ion (*m*/*z*) peak spectrum was recorded by ESI positive mode. A base peak was found for an isotopic abundance of gelator [$C_{18}H_{18}N_4O_4$]:

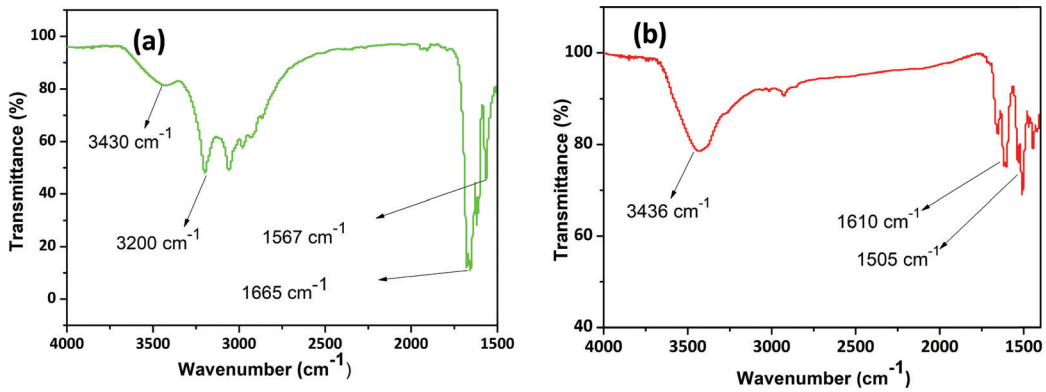

Fig. 2 FT-IR analysis of the gelator (a) and the xerogel (b), showing the coordination of Cu^{2+} through O, N, O linkages.

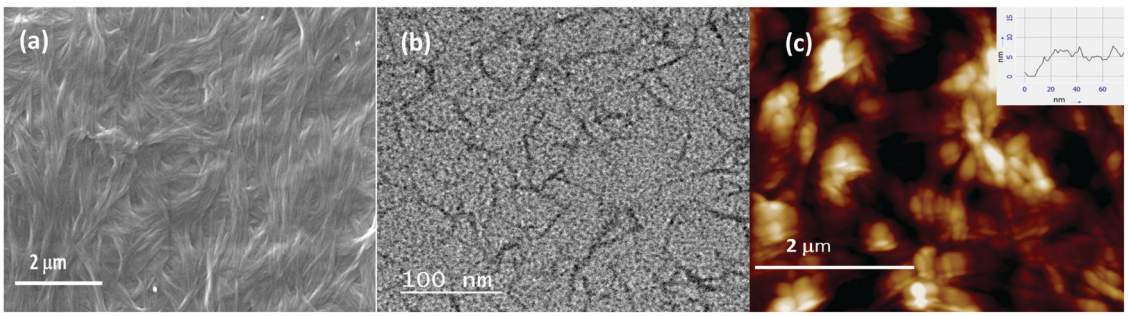

Fig. 3 (a) An SEM image of the vacuum-dried metallogel. (b) TEM and (c) AFM images of the metallogel ($H_4L/Cu(OAc)_2$; $\sim 10^{-3}$ M).

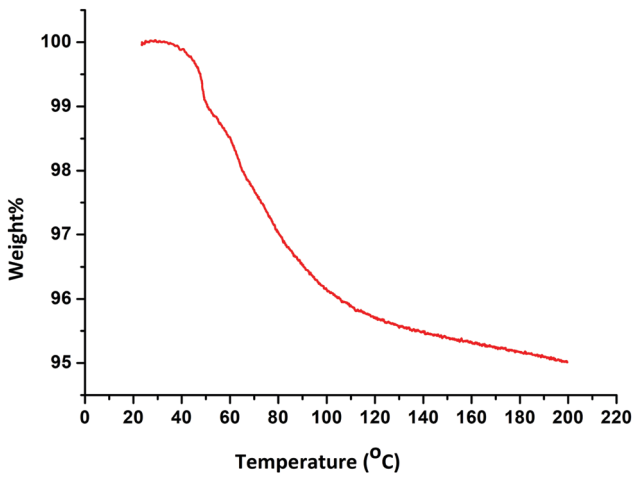

Fig. 4 The TGA curve of the xerogel from the Cu(II)–H_4L metallogel.

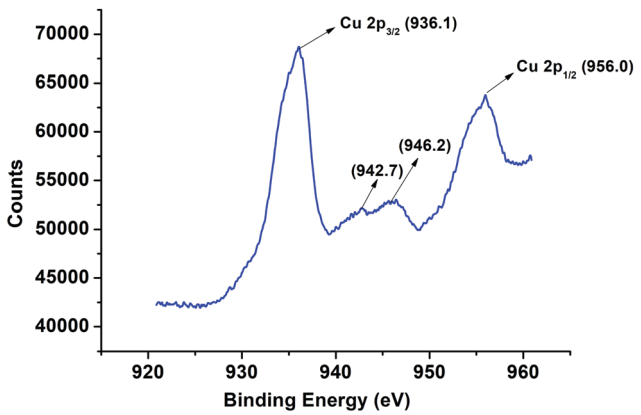

Fig. 5 The high-resolution Cu 2p XPS spectrum of the synthesized xerogel.

354.2, and its calculated base peak was observed at m/z 354.1. However, the base peak for diluted metallogel $[C_{18}H_{16}CuN_4O_4]^{2-}$ was found at m/z 415.2 and its estimated peak was at 415.1. Therefore, the molecular ion abundance pattern of ESI-MS spectra is smoothly matched with the calculated peak. The molecular abundance pattern of the metallogel well matched with a 1 : 1 proposed coordination mechanism between H_2L^{2-} and Cu^{2+} based on Job's plot and UV-visible study.

3.5. Rheological analysis

A semi-solid nature with viscoelasticity of the Cu based metallogel was confirmed by a rheological study such as angular frequency and strain sweep studies. The storage modulus (G') and loss modulus (G'') measurements of the gel are directly associated with the function of shear strain and shear stress, respectively, at 25 °C and a frequency of 10 rad s^{-1}. In the viscoelastic region, G' of the metallogel showed the stored energy in the system during the application of shear.

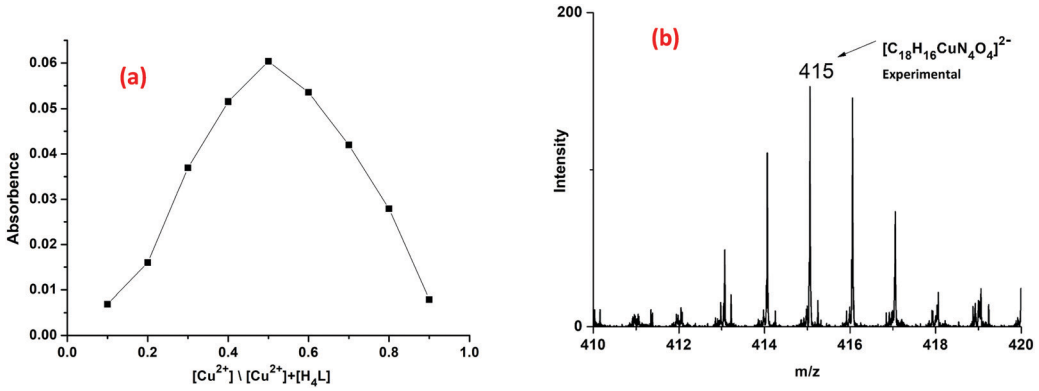

Fig. 6 (a) A Job plot showing [Cu(II)]/[Cu(II)] + [gelator] *vs.* absorbance monitored at 380 nm. (b) The ESI-MS spectrum of $[C_{18}H_{16}CuN_4O_4]$, presenting the experimental isotopic abundance pattern for 1 : 1 H_4L *vs.* Cu^{2+}.

For a liquid-like sample, G'' indicates energy change during dissolution under oscillatory stress.[32] The rheological experiment showed that G' of the Cu-based metallogel was higher than G'' by an order of ~1 of shear stress at a fixed concentration of the gel (Fig. 7). We have also observed that the value of shear stress of G' and G'' intersect at the point ~1.9 Pa. This point is the gel destruction point, which is known as a gel–sol transition point. A frequency sweep measurement was conducted between 0.1 and 100 rad s^{-1}. The viscoelastic value of the gel was in the range of 10^{-1} to 10^{2} rad s^{-1}, indicating that G' and G'' values increase linearly with increasing applied frequency. This result exhibited the elastic nature of gel. As shown in Fig. 7, it was observed that the value of $G' > G''$, which indicates the retention of the structural property of the Cu–H_4L metallogel.

3.6. Optical characterization

The optical characteristics were probed by UV-visible spectroscopy. The UV-visible spectrum (solid state) of a thin film of the Cu–H_4L metallogel was recorded in the range 250–600 nm. The calculation of the direct optical band gap of thin-film Cu–H_4L metallogel was performed using Tauc's equation:[20,33]

$$(\alpha h\nu)^2 = A(h\nu - E_g) \quad (1)$$

where E_g, h, α and ν stand for optical bandgap, Planck's constant, absorption coefficient, and frequency of light, respectively. Parameter A, which is unity in an ideal case, is a constant. With the extrapolation of the linear region of a plot of $(\alpha h\nu)^2$ *vs.* $h\nu$ (Fig. 8) to $\alpha = 0$ absorption, the direct optical band gap (E_g) was evaluated as 3.06 eV for the Cu–H_4L metallogel.

3.7. Strategy for device fabrication

By using the above optical properties of the synthesized metallogel, a Schottky diode was designed, as shown in Scheme 2.

It is evident from the Taucs plot analysis (Fig. 8) that our synthesized organo-metallogel (Cu–H_4L) is a semiconducting-range material. Hence, we have fabricated a metal (Ag)–semiconductor (Cu–H_4L) junction based thin-film device and investigated the current–voltage (I–V) characteristics of the device. The I–V measurements of the organo-metallogel (Cu–H_4L) based thin-film device were conducted with the help of the semiconductor parameter analyzer at a bias voltage from −2 V to +2 V at RT. I–V characteristics of fabricated devices have been examined, as shown in Fig. 9. By using the I–V characteristics of the Ag/Cu–H_4L based thin-film device, the interface between Ag and Cu–H_4L exhibits a nonlinear rectifying behaviour, which indicates the formation of a Schottky diode. The obtained I–V characteristics of the semiconductor gel at RT were further analyzed by assuming the standard thermionic theory and Cheung's equation[34–36] and we calculated key parameters of the fabricated device. To analyze the I–V graph, we first employed the

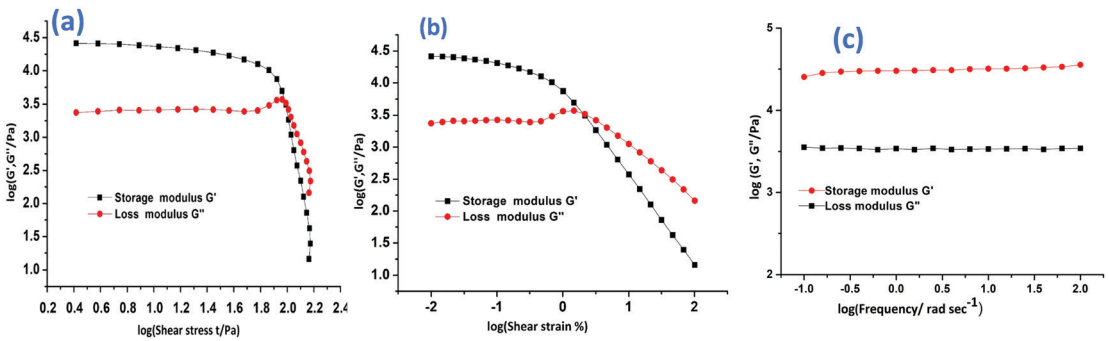

Fig. 7 (a) Dynamic shear stress against G'' and G'. (b) Dynamic oscillation strain *vs.* G'' and G'. (c) Frequency sweep measurements of G'' and G'.

following standard equation:

$$I = I_0 \exp\left(\frac{qV}{\eta' KT}\right)\left(1 - \exp\left(\frac{-qV}{\eta' KT}\right)\right) \quad (2)$$

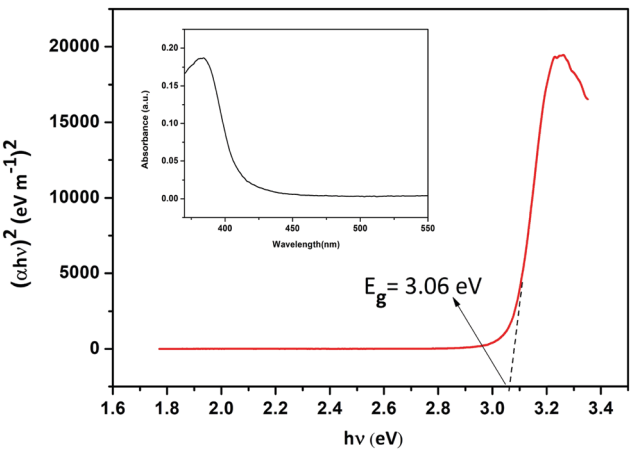

Fig. 8 The UV-visible absorption spectrum (inset) and Tauc plot for Cu–H_4L.

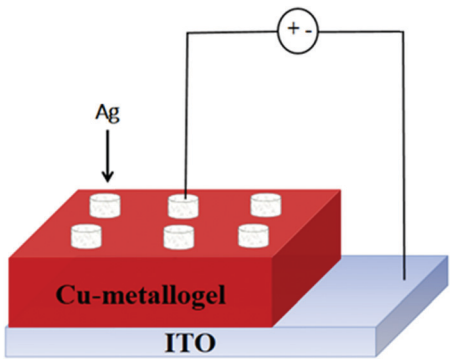

Scheme 2 A schematic representation of the fabrication of a Schottky diode based on the synthesized Cu–H_4L metallogel.

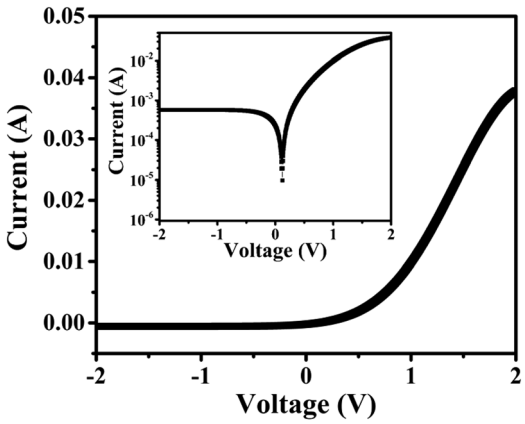

Fig. 9 *I–V* characteristic graph for the ITO/Cu–H_4L/Ag-based thin-film device.

Table 1 A comparison table including the charge transport parameters of the Ag/Cu–H_4L device

Device name	ON/OFF ratio	Series resistance (Ω)	Barrier height (eV)	Ideality factor	Ref.
Fe@MEA	375	13.9	0.72	1.33	38
$[Cd_4L_2(NCO)_6]_n$	12.44	5306	0.52	3.45	39
$C_{40}H_{34}Cu_2N_6O_{18}$	8.46	81.7	0.47	2.78	40
Au/CuO/P-Si/Al	—	410	0.79	1.58	41
Cu/ZnO	—	—	0.67	1.99	42
Ag/Cu–H_4L	70	65	0.61	3.0	**Present work**

$$I_0 = AA^* T^2 \exp\left(\frac{-q\phi_B}{KT}\right) \quad (3)$$

where I_0, q, K, T, V, A, η and A^* represent reverse saturation current, electronic charge, Boltzmann constant, temperature (K), voltage, effective diode area, ideality factor and Richardson constant, respectively. The effective diode area was calculated as 0.0314 cm^2 and the Richardson constant was considered as 32 A K^{-2} cm^{-2} for the Cu–H_4L gel based devices.

We have also calculated the series resistance (R_s), ideality factor (η') and barrier height (ϕ_B) by using following equations:

$$\frac{dV}{d(\ln I)} = \left(\frac{\eta' KT}{q}\right) + IR_s \quad (4)$$

$$\phi_B = \frac{KT}{q} \ln\left(\frac{A^* T^2}{J_0}\right) \quad (5)$$

The estimated value of reverse saturation current was 3.80×10^{-6} A and values of the calculated barrier height (ϕ_B), ideality factor (η), opening voltage (V) and series resistance (R_s) for the synthesized complex-based SBD respectively are ~0.61 eV, ~3.0, ~0.5 volts and ~65 Ω (Table 1). For a better understanding of the charge transport phenomena in the fabricated device, we analyzed the logarithmic-scale *I–V* characteristics which are shown in Fig. 10, which can be divided into two slopes defined as region-I and region-II. In region-I, current follows a linear behavior with voltage which corresponds to the

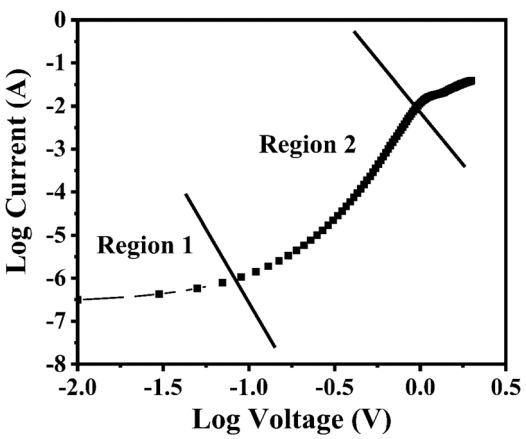

Fig. 10 log *I* *vs.* log *V* curve for the ITO/Cu–H_4L/Ag-based thin-film device.

ohmic regime. In region-II, current follows a nonlinear behavior with voltage and current is proportional to V^2. This corresponds to the trap free space charge limited current (SCLC) region.[37]

4. Conclusions

Herein, we have developed the practical synthesis of a new modular and functional metallogel, based on a succinic acid derivative and $Cu(OAc)_2$ in DMF. The gel-phase material was confirmed based on rheological experiments and also established was the mechanical stability of the metallogel. Well-defined cross-linked nanofibers of the supramolecular Cu^{2+}-based metallogel were confirmed *via* SEM, TEM, and AFM analyses. FT-IR, UV-visible, ESI-MS and Job plot results established the mechanism of the metallogel. The optical band-gap measurements of the metallogel based on the succinic acid-derived compound (H_4L) and $Cu(OAc)_2$ suggest the semiconducting nature of the metallogel. Additionally, we fabricated an MS junction thin-film electronic device from Ag metal and the semiconducting Cu–H_4L gel. The nonlinear charge transportation of the device obtained from the *I–V* characteristic graph confirmed the fabrication of a Schottky diode. Thus, the present study of ITO/Cu–H_4L/Ag suggests the future possibility of achieving supramolecular Cu^{2+} metallogel based electronic devices for advanced technology.

Conflicts of interest

There are no conflicts to declare.

Acknowledgements

The present work is financially supported by the IIT (BHU), Varanasi and MHRD, New Delhi, India. The authors are grateful to the CIFC, IIT (BHU) and Department of Chemistry, IIT (BHU) for providing the instrumentation facilities. The authors are also grateful to Mayank Varshney, Manoj Sharma, and Anton Paar for providing the rheological facilities.

References

1 K. Gao, Z. Zhang, L. Ma, L. Chen, X. Chen, Y. Zhang and M. Zhang, *Giant*, 2020, **4**, 100034.
2 Y. X. Ye, W. L. Liu and B. H. Ye, *Catal. Commun.*, 2017, **89**, 100–105.
3 F. A. Denis, P. Hanarp, D. S. Sutherland and Y. F. Dufrêne, *Langmuir*, 2004, **20**, 9335–9339.
4 W. Zhang, Z. Wang, L. Tao, K. Duan, H. Wang, J. Zhang, X. Pan and Z. Huo, *J. Solid State Electrochem.*, 2019, 1563–1570.
5 S. Bhowal, A. Ghosh, S. P. Chowdhuri, R. Mondal and B. B. Das, *Dalton Trans.*, 2018, **47**, 6557–6569.
6 G. Liu, J. Sheng, W. L. Teo, G. Yang, H. Wu, Y. Li and Y. Zhao, *J. Am. Chem. Soc.*, 2018, **140**, 16275–16283.
7 J. Jagur-Grodzinski, *Polym. Adv. Technol.*, 2010, **21**, 27–47.
8 A. Biswas, S. Mukhopadhyay, R. S. Singh, A. Kumar, N. K. Rana, B. Koch and D. S. Pandey, *ACS Omega*, 2018, **3**, 5417–5425.
9 N. Malviya, C. Sonkar, R. Ganguly, D. Bhattacherjee, K. P. Bhabak and S. Mukhopadhyay, *ACS Appl. Mater. Interfaces*, 2019, **11**, 47606–47618.
10 V. Van Tran, D. Park and Y. C. Lee, *Environ. Sci. Pollut. Res.*, 2018, **25**, 24569–24599.
11 Q. Lin, T. T. Lu, X. Zhu, B. Sun, Q. P. Yang, T. B. Wei and Y. M. Zhang, *Chem. Commun.*, 2015, **51**, 1635–1638.
12 S. Dhibar, A. Dey, S. Majumdar, A. Dey, P. P. Ray and B. Dey, *Ind. Eng. Chem. Res.*, 2020, **59**, 5466–5473.
13 S. Saha, E. M. Schön, C. Cativiela, D. Díaz Díaz and R. Banerjee, *Chem. – Eur. J.*, 2013, **19**, 9562–9568.
14 S. Ganta and D. K. Chand, *Inorg. Chem.*, 2018, **57**, 3634–3645.
15 S. Dhibar, A. Dey, A. Dey, S. Majumdar, D. Ghosh, P. P. Ray and B. Dey, *ACS Appl. Electron. Mater.*, 2019, **1**, 1899–1908.
16 R. Jana, A. Dey, M. Das, J. Datta, P. Das and P. P. Ray, *Appl. Surf. Sci.*, 2018, **452**, 155–164.
17 H. Sheng, S. Muthukumar, N. W. Emanetoglu and Y. Lu, *Appl. Phys. Lett.*, 2002, **80**, 2132–2134.
18 R. Borthakur, A. Kumar, A. Lemtur and R. A. Lal, *RSC Adv.*, 2013, **3**, 15139–15147.
19 R. K. Upadhyay, A. P. Singh, D. Upadhyay, S. Ratan, C. Kumar and S. Jit, *IEEE Photonics Technol. Lett.*, 2019, **31**, 1151–1154.
20 R. K. Upadhyay, A. P. Singh, D. Upadhyay, A. Kumar, C. Kumar and S. Jit, *IEEE Electron Device Lett.*, 2019, **40**, 1961–1964.
21 M. Sutradhar, T. Roy Barman, J. Kxlanke, M. G. B. Drew and E. Rentschler, *Polyhedron*, 2013, **53**, 48–55.
22 L. Wang, W. Qin, X. Tang, W. Dou and W. Liu, *J. Phys. Chem. A*, 2011, **115**, 1609–1616.
23 J. D. Ranford, J. J. Vittal and Y. M. Wang, *Inorg. Chem.*, 1998, **37**, 1226–1231.
24 M. Cametti, M. Cetina and Z. Džolić, *Dalton Trans.*, 2015, **44**, 7223–7229.
25 X. Wang, T. He, L. Yang, H. Wu, R. Zhang, Z. Zhang, R. Shen, J. Xiang, Y. Zhang and C. Wei, *Nanoscale*, 2016, **8**, 6479–6483.
26 V. K. Singh, V. Singh, P. K. Yadav, S. Chandra, D. Bano, V. Kumar, B. Koch, M. Talat and S. H. Hasan, *New J. Chem.*, 2018, **42**, 12990–12997.
27 S. Chandra, V. K. Singh, P. K. Yadav, D. Bano, V. Kumar, V. K. Pandey, M. Talat and S. H. Hasan, *Anal. Chim. Acta*, 2019, **1054**, 145–156.
28 F. Rezaei, R. Yunus and N. A. Ibrahim, *Mater. Des.*, 2009, **30**, 260–263.
29 A. Upadhyay, A. Narula and C. P. Rao, *ACS Appl. Bio Mater.*, 2020, **12**, 8619–8626.
30 D. Bano, S. Chandra, P. K. Yadav, V. K. Singh and S. H. Hasan, *J. Photochem. Photobiol., A*, 2020, **398**, 112558.

31 P. K. Yadav, V. K. Singh, S. Chandra, D. Bano, V. Kumar, M. Talat and S. H. Hasan, *ACS Biomater. Sci. Eng.*, 2019, **5**, 623–632.
32 S. Dhibar, A. Dey, R. Jana, A. Chatterjee, G. K. Das, P. P. Ray and B. Dey, *Dalton Trans.*, 2019, **48**, 17388–17394.
33 S. Dhibar, A. Dey, D. Ghosh, S. Majumdar, A. Dey, P. P. Ray and B. Dey, *ACS Omega*, 2020, **6**, 2680–2689.
34 S. K. Cheung and N. W. Cheung, *Appl. Phys. Lett.*, 1986, **49**, 85–87.
35 A. Dey, A. Layek, A. Roychowdhury, M. Das, J. Datta, S. Middya, D. Das and P. P. Ray, *RSC Adv.*, 2015, **5**, 36560–36567.
36 S. Dhibar, A. Dey, S. Majumdar, D. Ghosh, A. Mandal, P. P. Ray and B. Dey, *Dalton Trans.*, 2018, **47**, 17412–17420.
37 A. Dey, S. Middya, R. Jana, M. Das, J. Datta, A. Layek and P. P. Ray, *J. Mater. Sci.: Mater. Electron.*, 2016, **27**, 6325–6335.
38 S. Dhibar, R. Jana, P. P. Ray and B. Dey, *J. Mol. Liq.*, 2019, **289**, 111126.
39 P. Ghorai, A. Dey, P. Brandão, J. Ortega-Castro, A. Bauza, A. Frontera, P. P. Ray and A. Saha, *Dalton Trans.*, 2017, **46**, 13531–13543.
40 A. Hossain, A. Dey, S. K. Seth, P. P. Ray, P. Ballester, R. G. Pritchard, J. Ortega-Castro, A. Frontera and S. Mukhopadhyay, *ACS Omega*, 2018, **3**, 9160–9171.
41 S. Çetinkaya, H. A. Çetinkara, F. Bayansal and S. Kahraman, *Sci. World J.*, 2013, DOI: 10.1155/2013/126982.
42 A. Khan, M. Hussain, M. A. Abbasi, Z. H. Ibupoto, O. Nur and M. Willander, *Semicond. Sci. Technol.*, 2013, **12**, DOI: 10.1088/0268-1242/28/12/125006.

